

Time Delay in Strong Field Limit Gravitational Lensing

V. Bozza^{a,b,c}, L. Mancini^{b,c,d}

^a Centro studi e ricerche “Enrico Fermi”, Rome, Italy.

^b Dipartimento di Fisica “E. R. Caianiello”, Università di Salerno, 84081 Baronissi, Italy.

^c Istituto Nazionale di Fisica Nucleare, Sezione di Napoli, Italy.

^d Institut für Theoretische Physik der Universität Zürich, CH-8057 Zürich, Switzerland.

(Dated: May 22, 2019)

We calculate the time delay between different relativistic images formed by black hole gravitational lensing in the strong field limit. We show that different types of black holes are characterized by different time delays, so that one further quantity can eventually become available for the classification of black holes and a more precise determination of their parameters. The time delay for the black hole at the center of our Galaxy is few minutes, but for supermassive black holes with $M = 10^9 M_\odot$ in the neighbourhood of the Local Group the time delay amounts to few days, thus being measurable in principle.

PACS numbers: 95.30.Sf, 04.70.Bw, 98.62.Sb

Keywords: Relativity and gravitation; Classical black holes; Gravitational lensing

I. INTRODUCTION

Gravitational lensing turns out to be an useful tool to investigate a lot of aspects of the nature of the universe. It was the first prove of the validity of the theory of general relativity (GR) [1], and today its effects in extragalactic scale (lensing of quasars, arcs in galaxy clusters, etc.) and in galactic scale (microlensing) are ordinarily observed and studied by the scientific community in weak field approximation [2].

In the last years, a new form of gravitational lensing has been proposed as a method to investigate the gravitational field generated by collapsed objects. This approach considers light rays of background sources passing very close to the event horizons of black holes without entering inside. The study of this extreme case is of remarkable interest: on one hand a new prove of the validity of all GR could arise, on the other hand intrinsic features of the lens (rotation, electric charge, etc.) could become accessible to the observations.

In Schwarzschild framework, a light ray with small impact parameter can wind several times around a black hole without being definitively caught inside. In this way, a set of infinite relativistic images can be generated on each side of the black hole [3, 4, 5]. In Ref. [6] analytical formulae for the position and the magnification of the images were obtained, defining a *strong field limit* for the deflection angle. These formulae were applied to a Reissner-Nordstrom black hole in Ref. [7], and were also used to calculate relativistic effects on microlensing events [8]. A full generalization of the strong field limit for any spherically symmetric spacetime was drawn in Ref. [9] and applied to several black hole metrics, allowing a non-degenerate discrimination among different collapsed objects. Finally, in work [10] the case of a Kerr black hole and the relevance of its spin in strong field lensing approximation was discussed for light rays travelling on quasi-equatorial trajectories.

When multiple images are formed, the light-travel-time

along light paths corresponding to different images is generally not the same. So, luminosity variations of the source would reach the observer with a relative temporal phase depending on the geometry of the lens [11]. These time delays can be measured. In gravitational lensing experiments, the time delay of the images is one of the most important quantities because it is the only dimensional observable. Therefore its measurement is useful to determine at first the length scale for a gravitational lensing system and its mass. In a cosmological context, it is possible to determine the cosmological distance scale and hence the Hubble parameter [11, 12, 13]. This fact has drawn a great attention by the scientific community towards this kind of measurements.

In the present paper, we estimate the time delay between images generated by strong field lensing due to different types of black holes. Our aim is to show that the difference among time delays helps to distinguish and classify black holes. Our method is particularly efficient to study extragalactic black holes, where the time delay of the images is easily appreciable.

This paper is structured as follows. In Sect. 2, we recall the main results of the strong field limit method and derive the general form for the time delay. In Sect. 3, we apply this method to some spherically symmetric metrics (Schwarzschild, Reissner-Nordstrom, Janis-Newman-Winicour) and to Kerr metric. Then, in Sect 4, we estimate the expected time delays for several interesting supermassive extragalactic black holes. Finally, in Sect. 5, we discuss the physical aspects and draw the conclusions.

II. TIME DELAY IN THE STRONG FIELD LIMIT

The technique we use in the derivation of the time delay between different images resembles the main calculation of the deflection angle in the strong field limit

approach. We shall briefly recall the main steps of that derivation referring the reader to Refs. [9, 10] for all the details.

A. The strong field limit approach

Consider a generic black hole metric projected on the equatorial plane

$$ds^2 = A(x)dt^2 - B(x)dx^2 - C(x)d\phi^2 + D(x)dt d\phi \quad (1)$$

where $D(x)$ can be consistently set to zero in a spherically symmetric black hole.

The metric does not depend on time and the azimuthal angle ϕ , so that, for a photon moving in this background, t and ϕ can be expressed in terms of two integrals of motion, namely energy and angular momentum. By a suitable choice of the affine parameter, we set the first to 1 and the second to the impact parameter u of the incoming photon. We have

$$\dot{t} = \frac{4C - 2uD}{4AC + D^2} \quad (2)$$

$$\dot{\phi} = \frac{4Au + 2D}{4AC + D^2}. \quad (3)$$

The impact parameter u , is related to the closest approach distance x_0 by

$$u = \frac{-D_0 + \sqrt{4A_0C_0 + D_0^2}}{2A_0}, \quad (4)$$

where all functions with the subscript 0 are evaluated for $x = x_0$.

By the on-shell condition for the photon, we also derive

$$\dot{x} = \pm \frac{2}{\sqrt{B}} \sqrt{\frac{C - uD - u^2A}{4AC + D^2}}. \quad (5)$$

Dividing Eq. (3) by Eq. (5), we get

$$\frac{d\phi}{dx} = P_1(x, x_0)P_2(x, x_0) \quad (6)$$

$$P_1(x, x_0) = \frac{\sqrt{B}(2A_0Au + A_0D)}{\sqrt{CA_0}\sqrt{4AC + D^2}} \quad (7)$$

$$P_2(x, x_0) = \frac{1}{\sqrt{A_0 - A\frac{C_0}{C} + \frac{u}{C}(AD_0 - A_0D)}}. \quad (8)$$

Integrating this expression from x_0 to infinity we find half the deflection angle as a function of the closest approach. Given the symmetry between approach and departure, we can write the whole deflection angle as

$$\alpha(x_0) = \phi_f(x_0) - \pi \quad (9)$$

$$\phi_f(x_0) = 2 \int_{x_0}^{\infty} \frac{d\phi}{dx} dx. \quad (10)$$

To solve this integral, we define the variables

$$y = A(x) \quad (11)$$

$$z = \frac{y - y_0}{1 - y_0} \quad (12)$$

where $y_0 \equiv A_0$. The integral (10) in the deflection angle becomes

$$\phi_f(x_0) = \int_0^1 R(z, x_0) f(z, x_0) dz \quad (13)$$

$$R(z, x_0) = 2 \frac{1 - y_0}{A'(x)} P_1(x, x_0) \quad (14)$$

$$f(z, x_0) = P_2(x, x_0) \quad (15)$$

where $x = A^{-1} [(1 - y_0)z + y_0]$.

The function $R(z, x_0)$ is regular for all values of z and x_0 , while $f(z, x_0)$ diverges for $z \rightarrow 0$. We then expand the argument of the square root in $f(z, x_0)$ to the second order in z , defining

$$f(z, x_0) \sim f_0(z, x_0) = \frac{1}{\sqrt{\alpha z + \beta z^2}}. \quad (16)$$

The Eq. $\alpha = 0$ defines the radius of the photon sphere x_m , which is the minimum approach distance for photons not falling into the black hole.

The result of the integral (13) gives the strong field limit expansion of the deflection angle [9]

$$\alpha(u) = -\bar{a} \log \left(\frac{u}{u_m} - 1 \right) + \bar{b} + O(u - u_m), \quad (17)$$

where the coefficients of the expansion are

$$u_m = \frac{-D_m + \sqrt{4A_mC_m + D_m^2}}{2A_m} \quad (18)$$

$$\bar{a} = \frac{R(0, x_m)}{2\sqrt{\beta_m}} \quad (19)$$

$$\bar{b} = -\pi + b_D + b_R + \bar{a} \log \frac{cx_m^2}{u_m} \quad (20)$$

and

$$b_D = 2\bar{a} \log \frac{2(1 - y_m)}{A'_m x_m} \quad (21)$$

$$b_R = \int_0^1 [R(z, x_m) f(z, x_m) - R(0, x_m) f_0(z, x_m)] dz, \quad (22)$$

while c is defined by the expansion

$$u - u_m = c(x_0 - x_m)^2. \quad (23)$$

All the functions with the subscript m are evaluated at $x_0 = x_m$.

With the formula (17) for the deflection angle, it is straightforward to calculate the positions and the magnifications of all relativistic images. Two infinite patterns of relativistic images appear on each side of the lens, very close to the minimum impact angle $\theta_m = u_m/D_{OL}$ (D_{OL} is the distance of the lens from the observer). These images are highly demagnified unless the source is very close to a caustic point. For spherically symmetric black holes, all caustic points are exactly aligned with the lens, so that a source aligned with the optical axis (the line joining observer and lens) would enhance the magnification of all images simultaneously.

In spinning black holes, the caustics drift away from the optical axis, so that one source cannot be simultaneously close to different caustics. In this case only one image at a time can be enhanced while all others stay very faint [10]. Nevertheless, in this case, additional images, appearing when the source is inside a caustic, may play an important role in the phenomenology, yet to be understood.

For later reference, we write here the formula for the position of the relativistic images

$$\theta_n^\pm = \pm \theta_m \left(1 + e^{\frac{\bar{b} - 2n\pi \pm \gamma}{\pi}} \right). \quad (24)$$

Here γ is the angular separation between the source and the optical axis, as seen from the lens. n is the number of loops done by the photon around the black hole. For each n , we have an image on each side of the lens, according to the chosen sign.

B. Time delay computation

In this subsection we shall derive the time delay between different relativistic images, following an approach very similar to the one reported in the previous subsection for the deflection angle.

For an observer at infinity, the time taken from the photon to travel from the source to the observer is simply

$$T = \int_{t_0}^{t_f} dt. \quad (25)$$

Changing the integration variable from t to x , we split the integral into approach and leaving phases

$$T = \int_{D_{LS}}^{x_0} \frac{dt}{dx} dx + \int_{x_0}^{D_{OL}} \frac{dt}{dx} dx. \quad (26)$$

Here D_{LS} is the distance between the source and the lens, while D_{OL} is the distance between the lens and the observer.

Extending the integration limits to infinity, we can unify the two integrals into one, exploiting the symmetry

between approach and departure. This can be done at the price of subtracting two terms

$$T = 2 \int_{x_0}^{\infty} \left| \frac{dt}{dx} \right| dx - \int_{D_{OL}}^{\infty} \left| \frac{dt}{dx} \right| dx - \int_{D_{LS}}^{\infty} \left| \frac{dt}{dx} \right| dx. \quad (27)$$

If we consider two photons, travelling on different trajectories, the time delay between them is

$$\begin{aligned} T_1 - T_2 = & 2 \int_{x_{0,1}}^{\infty} \left| \frac{dt}{dx}(x, x_{0,1}) \right| dx - 2 \int_{x_{0,2}}^{\infty} \left| \frac{dt}{dx}(x, x_{0,2}) \right| dx \\ & - \int_{D_{OL}}^{\infty} \left| \frac{dt}{dx}(x, x_{0,1}) \right| dx + \int_{D_{OL}}^{\infty} \left| \frac{dt}{dx}(x, x_{0,2}) \right| dx \\ & - \int_{D_{LS}}^{\infty} \left| \frac{dt}{dx}(x, x_{0,1}) \right| dx + \int_{D_{LS}}^{\infty} \left| \frac{dt}{dx}(x, x_{0,2}) \right| dx. \end{aligned} \quad (28)$$

Supposing that observer and source are very far from the black hole, dt/dx is effectively 1 in the last four integrals which thus exactly cancel each other. We are thus left with the first two integrals.

Dividing Eq. (2) by Eq. (5), we obtain

$$\frac{dt}{dx} = \tilde{P}_1(x, x_0) P_2(x, x_0) \quad (29)$$

$$\tilde{P}_1(x, x_0) = \frac{\sqrt{BA_0}(2C - uD)}{\sqrt{C}\sqrt{4AC + D^2}} \quad (30)$$

and P_2 defined by Eq. (8). Of course, dt/dx tends to one for large x and the two integrals in (28) are separately divergent, while their difference is finite. In fact, the time delay is the result of the different paths followed by the photons while they wind around the black hole. When the two photons are far away from the black hole, $dt/dx \rightarrow 1$ and the two integrals compensate each other. Separating the two regimes, we can write individually convergent integrals. To achieve this, we subtract and add the function $\tilde{P}_1(x, x_{0,i})/\sqrt{A_{0,i}}$ to each integrand. Supposing $x_{0,1} < x_{0,2}$, we can write

$$\begin{aligned} T_1 - T_2 = & \tilde{T}(x_{0,1}) - \tilde{T}(x_{0,2}) + 2 \int_{x_{0,1}}^{x_{0,2}} \frac{\tilde{P}_1(x, x_{0,1})}{\sqrt{A_{0,1}}} dx \\ & + 2 \int_{x_{0,2}}^{\infty} \left[\frac{\tilde{P}_1(x, x_{0,1})}{\sqrt{A_{0,1}}} - \frac{\tilde{P}_1(x, x_{0,2})}{\sqrt{A_{0,2}}} \right] dx \end{aligned} \quad (31)$$

with

$$\tilde{T}(x_0) = \int_0^1 \tilde{R}(z, x_0) f(z, x_0) dz \quad (32)$$

$$\tilde{R}(z, x_0) = 2 \frac{1 - y_0}{A'(x)} \tilde{P}_1(x, x_0) \left(1 - \frac{1}{\sqrt{A_0} f(z, x_0)} \right) \quad (33)$$

and $f(x, x_0)$ defined by Eq. (15). Substituting all the expressions back into (31), we can check that it is equivalent to (28), but now it is written as a sum of separately convergent integrals.

In practice, the integral $\tilde{T}(x_0)$ represents the time spent by the light ray to wind around the black hole. In order to cutoff the integrands at large x 's, in the definition of $R(z, x_0)$ we have subtracted a term which is negligible when the photon is close to the black hole but cancels the integrand when the photon is far from the black hole. The residual terms of this subtraction are stored in the last two integrals in (31) and are generally subleading with respect to $\Delta\tilde{T}$, as we shall see later.

The integral (32) can be solved following the same technique of the integral (13) in the previous subsection, just replacing R by \tilde{R} . The result is

$$\tilde{T}(u) = -\tilde{a} \log \left(\frac{u}{u_m} - 1 \right) + \tilde{b} + O(u - u_m) \quad (34)$$

where u_m is defined by Eq. (18) and

$$\tilde{a} = \frac{\tilde{R}(0, x_m)}{2\sqrt{\beta_m}} \quad (35)$$

$$\tilde{b} = -\pi + \tilde{b}_D + \tilde{b}_R + \tilde{a} \log \frac{cx_m^2}{u_m} \quad (36)$$

with

$$\tilde{b}_D = 2\tilde{a} \log \frac{2(1 - y_m)}{A'_m x_m} \quad (37)$$

$$\tilde{b}_R = \int_0^1 \left[\tilde{R}(z, x_m) f(z, x_m) - \tilde{R}(0, x_m) f_0(z, x_m) \right] dz. \quad (38)$$

For spherically symmetric black holes, the expression for the time delay can be advantageously simplified. Notice that, for spherically symmetric spacetimes, $D = 0$ and

$$\tilde{P}_1(x, x_0)|_{D=0} = \sqrt{\frac{B A_0}{A}}. \quad (39)$$

Then the last integral in (31) identically vanishes. When $D \neq 0$, the dependence on x_0 remains through the impact parameter u which is present in Eq. (30). The second integral in (31) can be approximated substituting the integrand with $\sqrt{B_m/A_m}$ since it is practically constant throughout the (very small) integration interval. Finally, combining (34) with (17) we get a very simple expression for the first term in (31).

In writing the final formulae, we distinguish the case when the two images are on the same side of the lens from the case when the two images are on opposite sides of the lens. In the first case, we have

$$\Delta T_{n,m}^s = 2\pi(n - m) \frac{\tilde{a}}{\bar{a}} + 2\sqrt{\frac{B_m}{A_m}} \sqrt{\frac{u_m}{c}} e^{\frac{\tilde{b}}{2\bar{a}}} \left(e^{-\frac{2m\pi\mp\gamma}{2\bar{a}}} - e^{-\frac{2n\pi\mp\gamma}{2\bar{a}}} \right), \quad (40)$$

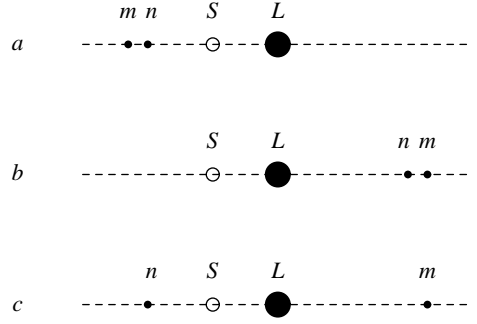


FIG. 1: This figure illustrates which images are considered in the different time delay calculations in the text. L represents the lens, S is the source. On each side of the lens an infinite series of images is formed. In case a , we consider two images on the same side of the source. Their time delay is given by $\Delta T_{n,m}^s$ with the upper sign. In case b , we consider two images appearing on the same side but opposite to the source. Their time delay is given by $\Delta T_{n,m}^s$ with the lower sign. Finally, in case c , we consider two images appearing on opposite sides. Their time delay is given by $\Delta T_{n,m}^o$.

where the upper sign before γ applies if both images are on the same side of the source (Fig. 1a) and the lower sign if both images are on the other side (Fig. 1b).

If the images are on opposite sides of the lens (Fig. 1c), then

$$\Delta T_{n,m}^o = [2\pi(n - m) - 2\gamma] \frac{\tilde{a}}{\bar{a}} + 2\sqrt{\frac{B_m}{A_m}} \sqrt{\frac{u_m}{c}} e^{\frac{\tilde{b}}{2\bar{a}}} \left(e^{-\frac{2m\pi-\gamma}{2\bar{a}}} - e^{-\frac{2n\pi+\gamma}{2\bar{a}}} \right), \quad (41)$$

where the image winding n times is on the same side of the source and the other is on the opposite side.

For spherically symmetric metrics, we also have the relation

$$\frac{\tilde{a}}{\bar{a}} = \frac{\sqrt{C_m}}{A_m} \quad (42)$$

which can be used to put Eqs. (40) and (41) in a more readable form in terms of the metric functions.

For physically reasonable values of the coefficients \bar{a} , \bar{b} , which are all of order one, the second term at the right hand side of Eq. (41) is much smaller than the first. Notice also that the geometry mostly favoured for the observation of relativistic images is that with the source almost aligned with the lens, so that $\gamma \sim D_{OL}^{-1} \ll 2\pi$. Therefore

$$\Delta T_{n,n}^o \ll T_{n,m \neq n}^s \simeq T_{n,m \neq n}^o \quad (43)$$

i.e. if we evaluate the time delay between images with the same winding number on opposite sides, we generally

find a value which is much smaller than the time delay between images with different winding number.

III. EXAMPLES

In this section, we implement the calculation described in the former section within three different spherically symmetric metrics: Schwarzschild, Reissner-Nordstrom, Janis-Newman-Winicour. Finally, we also examine the Kerr metric in equatorial lensing configuration.

A. Schwarzschild

Schwarzschild black hole lensing in the strong field limit was widely investigated in Refs. [6, 9]. Defining the Schwarzschild radius as the unit of distance ($2M = 1$), the metric functions are

$$A(x) = 1 - \frac{1}{x} \quad (44)$$

$$B(x) = \left(1 - \frac{1}{x}\right)^{-1} \quad (45)$$

$$C(x) = x^2 \quad (46)$$

$$D(x) = 0. \quad (47)$$

The radius of the photon sphere is

$$x_m = \frac{3}{2}. \quad (48)$$

The strong field limit coefficients for the deflection angle expansion are

$$u_m = \frac{3\sqrt{3}}{2} \quad (49)$$

$$\bar{a} = 1 \quad (50)$$

$$\bar{b} = -\pi + \log [216 (7 - 4\sqrt{3})] = -0.4. \quad (51)$$

Direct calculation of the coefficient \tilde{a} through Eq. (35) gives

$$\tilde{a} = \frac{3\sqrt{3}}{2}. \quad (52)$$

So each loop done by the photon around the black hole takes a time $2\pi(3\sqrt{3})/2$ for an observer at infinity. All loops have a radius very close to the radius of the photon sphere, but an additional $\sqrt{3}$ redshift factor arises to slow down the motion of the photon as perceived by an observer at infinity.

Now suppose that we observe the outermost images ($n = 1$ in (24)) and the second outermost images ($n = 2$) with a source almost perfectly aligned with the lens ($|\gamma| \ll 2\pi$), in order to have appreciably magnified images. Then the time delay between opposite images of same n will be negligible, while the time delay between

the second and the first images is the same, both if we consider images on the same side and if we consider images on opposite sides, the difference being of order γ . The result is

$$\Delta T_{2,1} = 16.57 \quad (53)$$

This result is given in Schwarzschild units. To obtain the time delay expressed in seconds, we must multiply for the Schwarzschild radius of our black hole in meters and divide by the light speed. The physical values range from few minutes to several days, depending on the black hole mass. Section IV contains a table of time delays for several interesting supermassive black holes and an extensive discussion about the observability of the time delay parameter.

We can also notice that the second term in formulae (40) and (41) contributes only 1.4% to the total time delay.

B. Reissner-Nordstrom

Now let us consider an electrically charged black hole, the metric being

$$A(x) = 1 - \frac{1}{x} + \frac{q^2}{x^2} \quad (54)$$

$$B(x) = \left(1 - \frac{1}{x} + \frac{q^2}{x^2}\right)^{-1} \quad (55)$$

$$C(x) = x^2 \quad (56)$$

$$D(x) = 0. \quad (57)$$

The radius of the photon sphere is

$$x_m = \frac{3}{4} \left(1 + \sqrt{1 - \frac{32q^2}{9}}\right). \quad (58)$$

The strong field limit coefficients are functions of the electric charge q

$$u_m = \frac{\left(3 + \sqrt{9 - 32q^2}\right)^2}{4\sqrt{2}\sqrt{3 - 8q^2 + \sqrt{9 - 32q^2}}} \quad (59)$$

$$\bar{a} = \frac{x_m \sqrt{x_m - 2q^2}}{\sqrt{(3 - x_m)x_m^2 - 9q^2x_m + 8q^4}} \quad (60)$$

$$\bar{b} = -\pi + b_R + \bar{a} \log 2 (x_m - q^2)^2 \times \times \frac{[(3 - x_m)x_m^2 - 9q^2x_m + 8q^4]}{(x_m - 2q^2)^3 (x_m^2 - x_m + q^2)}. \quad (61)$$

Similarly, we can calculate the coefficient \tilde{a} , required for the calculation of the time delay

$$\tilde{a} = \frac{x_m^3 \sqrt{x_m - 2q^2}}{\sqrt{x_m^2 - x_m + q^2} \sqrt{(3 - x_m)x_m^2 - 9q^2x_m + 8q^4}}. \quad (62)$$

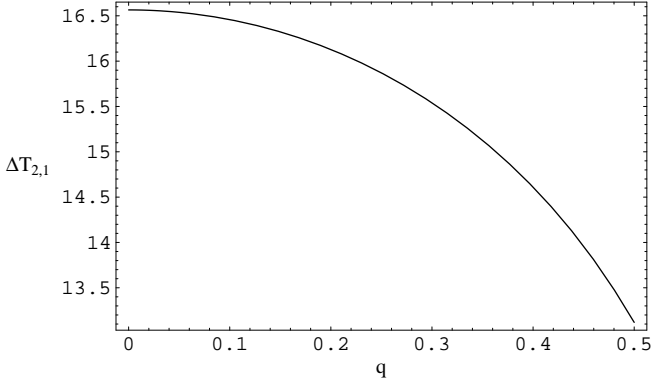


FIG. 2: Time delay between the second and the first relativistic images as a function of electric charge, normalized to the Schwarzschild radius $2M$.

In Fig. 2, we plot the time delay $\Delta T_{2,1}$ between the second and the first outermost images as a function of the electric charge. We clearly see that black holes with the same mass but different electric charges are characterized by different time delays. In particular, the time delay decreases with charge.

C. Janis-Newman-Winicour

The Janis-Newman-Winicour (JNW) metric describes the metric of a spherically symmetric object with mass M and charge q with respect to a massless scalar field [14]

$$A(x) = \left(1 - \frac{1}{x}\right)^\gamma \quad (63)$$

$$B(x) = \left(1 - \frac{1}{x}\right)^{-\gamma} \quad (64)$$

$$C(x) = \left(1 - \frac{1}{x}\right)^{1-\gamma} x^2 \quad (65)$$

$$\Phi(x) = \frac{q}{2\sqrt{M^2 + q^2}} \log\left(1 - \frac{1}{x}\right) \quad (66)$$

$$\gamma = \frac{M}{\sqrt{M^2 + q^2}}. \quad (67)$$

where all distances are measured in terms of $x_s = 2\sqrt{M^2 + q^2}$.

Here the radius of the photon sphere is

$$x_m = \frac{2\gamma + 1}{2} \quad (68)$$

and the strong field limit coefficients of the deflection

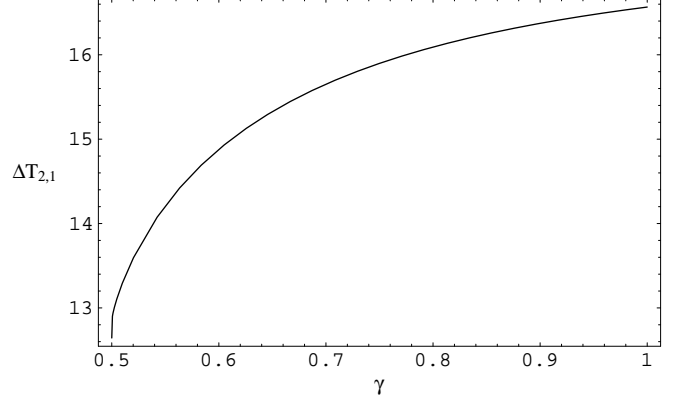


FIG. 3: Time delay between the second and the first relativistic images (normalized to the Schwarzschild radius $2M$) as a function of scalar charge in JNW metric.

angle are

$$u_m = \frac{(2\gamma + 1)^{\gamma + \frac{1}{2}}}{2(2\gamma - 1)^{\gamma - \frac{1}{2}}} \quad (69)$$

$$\bar{a} = 1 \quad (70)$$

$$\bar{b} = -\pi + b_R +$$

$$+ 2 \log \frac{[(2\gamma + 1)^\gamma - (2\gamma - 1)^\gamma]^2 (2\gamma + 1)}{2\gamma^2 (2\gamma - 1)^{2\gamma - 1}}. \quad (71)$$

The coefficient \tilde{a} for the time delay is

$$\tilde{a} = \frac{(2\gamma + 1)^{\gamma + 1/2}}{2(2\gamma - 1)^{\gamma - 1/2}}. \quad (72)$$

In Fig. 3, we plot the time delay $\Delta T_{2,1}$ between the second and the first outermost images as a function of the scalar charge. Here as well the time delay decreases with scalar charge.

D. Kerr

The Kerr metric projected on the equatorial plane reads

$$A(x) = 1 - \frac{1}{x} \quad (73)$$

$$B(x) = \frac{1}{1 - \frac{1}{x} + \frac{a^2}{x^2}} \quad (74)$$

$$C(x) = x^2 + a^2 + \frac{a^2}{x} \quad (75)$$

$$D(x) = 2\frac{a}{x}, \quad (76)$$

where a is the specific angular momentum of the black hole.

We cannot take advantage of all the simplifications of the spherically symmetric case, and we must start directly from Eq. (31). Yet we can still express the dominant term $\Delta \bar{T}$ in a simpler form. Consider first the case

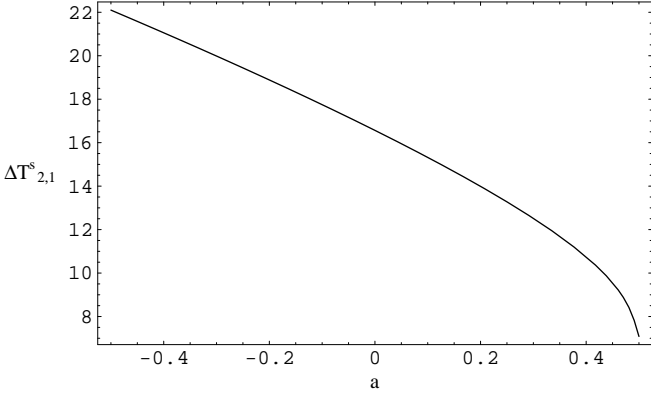


FIG. 4: Time delay (as a function of the black hole spin) between the second and the first relativistic images appearing on the same side of a Kerr black hole.

of two images on the same side of the black hole. Then everything works in the same way as for spherically symmetric black holes and we get

$$\Delta\tilde{T}_{n,m}^s = 2\pi(n-m)\frac{\tilde{a}}{\bar{a}}. \quad (77)$$

Of course, the values of \tilde{a} and \bar{a} depend on the sign of the spin a , i.e. they are different for photons winding in the same sense of the black hole (direct photons) and for photons winding in the opposite sense (retrograde photons).

If we wish to evaluate the time delay between two relativistic images appearing on opposite sides of the black hole, then we have to take care of the fact the one image will be direct and the other will be retrograde. We then get

$$\begin{aligned} \Delta\tilde{T}_{n,m}^o = & \frac{\tilde{a}(a)}{\bar{a}(a)}[2\pi n + \gamma - \bar{b}(a)] + \tilde{b}(a) - \\ & \frac{\tilde{a}(-a)}{\bar{a}(-a)}[2\pi m - \gamma - \bar{b}(-a)] - \tilde{b}(-a) \end{aligned} \quad (78)$$

and we see that now we also need the coefficients \bar{b} and \tilde{b} for the calculation, since they are not the same for the two images and do not cancel like in the spherically symmetric case.

Considering a source aligned behind the black hole ($\gamma = 0$), in Fig. 4 we plot the time delay between the second and first images appearing on the same side of the black hole. For positive a the two images are direct and for negative a they are both retrograde. We see that the time delay decreases if the images are both direct, while increases if they are both retrograde. We can also notice that the largest contribution to the time delay still comes from $\Delta\tilde{T}$, while the second term in (31) at most contributes for 6% when $a = 0.5$ and the last term stays below 0.7%.

The situation is quite different for images on opposite sides (Fig. 5). The time delay is zero when $a = 0$ and

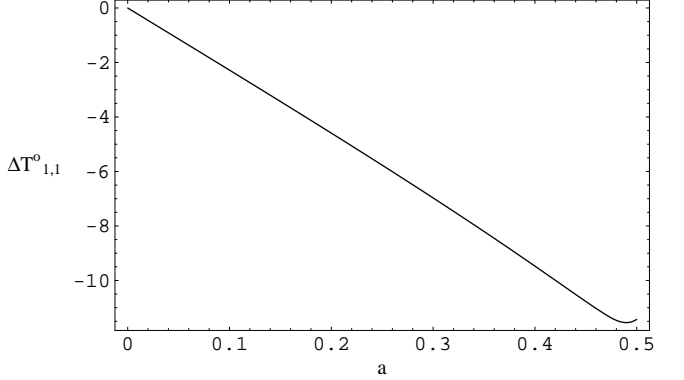


FIG. 5: Time delay (as a function of the black hole spin) between the first direct relativistic image and the first retrograde image.

becomes negative for positive a . This means that direct light rays take less time than retrograde rays to wind around the black hole. This is naturally understood since the radius of the photon sphere is larger for retrograde light rays. For high values of the black hole spin, $\Delta T_{1,1}^o$ becomes comparable to $\Delta T_{2,1}^s$. Another interesting fact is that the second term in (31) is of the same order of the dominant term $\Delta\tilde{T}$, the ratio being roughly $-1/3$. The last term also contributes for 1.7%.

IV. TIME DELAY IN SUPERMASSIVE BLACK HOLE LENSING

The important fact emerging from the application of our method to physical situations is that the gravitational lensing could be employed in an effective way to investigate the strong gravitational fields generated by collapsed objects of different types. This is true in the case we are able to distinguish at least the outermost relativistic image from the others. Yet, as noted in [9], in order to achieve this situation, we need an optical resolution one or two orders of magnitude better than that reachable by short-term VLBI projects [15]. However, we can be confident that relativistic images will possibly become a target for next generation projects.

In the previous section, we derived the time delay between different images formed by several kinds of black holes. The results have been presented in Schwarzschild units. Here we give realistic values for the time delay between the second and the first relativistic image and the range in which it varies, depending on the physical nature and, especially, the mass of the black hole. We treat only black holes with spherical symmetry, because only in this case we have the formation at first of more than one observable image. In fact, as noted in [10], the phenomenology of spinning black holes is quite different. In particular, if the source is not inside a caustic, only one image should become visible, while all the others stay

Local Group Galaxy	Mass (M_{\odot})	Distance (Mpc)	Schwarzschild $\Delta T_{2,1}$
Milky Way	2.8×10^6	0.0085	0.1 h
NGC0221 (M32)	3.4×10^6	0.7	0.2 h
NGC0224 (M31)	3.0×10^7	0.7	1.4 h

TABLE I: Estimates for the time delay for the supermassive black hole located at the centers of three galaxies in the case of Schwarzschild spacetime geometry. The masses and the distances are taken from Richstone et al. [16].

very faint. On the contrary, if the source is inside a caustic, two additional non-equatorial images should appear. But an analytical treatment for these additional images is not available at present.

Of course, we require also that the source must have temporal variations, otherwise there is no time delay to measure. Thus, an essential condition is that the source must be somehow variable. However, this is not a so restrictive requirement, since variable stars are generally abundant in all galaxies.

In Table I, we present the values of the time delay for the black hole located at the center of the Milky Way and in other two galaxies of the Local Group. The results are obtained using the Schwarzschild metric. It is clear that we have a little chance to observe such short time delays for reasonable times of exposure.

In order to have higher time delays, we need black holes with larger Schwarzschild radii, i.e. more massive black holes. At the same time we require that the magnification of the images must remain of the same order. Since we know that the magnification is proportional to $M_{\text{Lens}}/D_{\text{OL}}$, our request can be achieved if we consider lenses with a mass of two or three orders of magnitude larger than the black hole in the center of our galaxy, and located not farther than three orders of magnitude its distance. In this case, the measurement of the time delay becomes more favorable as shown in Tables II, III and IV, where we report our estimates for the time delay due to supermassive black holes located at the centers of not too far galaxies, according to spacetime geometry.

Following the strategy exposed in [9], we notice that the time delay could become an extra observable contributing to the identification of the physical features of the black holes. With one more observable it would be easier to constrain the parameters of the black holes (mass, electric charge, coupling to scalar fields, etc.) in a more efficient way. Moreover, it must be taken in consideration that a time delay can be measured, in principle, with a great precision. This would give an outstanding importance to time delay measurements in making a clearer classification of black holes.

Galaxy	Mass (M_{\odot})	Distance (Mpc)	Schwarzschild $\Delta T_{2,1}$
NGC4486 (M87)	3.3×10^9	15.3	149.3 h
NGC3115	2.0×10^9	8.4	90.5 h
NGC4374 (M84)	1.4×10^9	15.3	63.3 h
NGC4594 (M104)	1.0×10^9	9.2	45.2 h
NGC4486B (M104)	5.7×10^8	15.3	25.8 h
NGC4261	4.5×10^8	27.4	20.4 h
NGC4342 (IC3256)	3.9×10^8	15.3	17.6 h
NGC7052	3.3×10^8	58.7	14.9 h
NGC3377	1.8×10^8	9.9	8.1 h

TABLE II: Estimates for the time delay for supermassive black holes located at the center of several nearby galaxies in the case of Schwarzschild spacetime geometry. The masses and the distances of the central black holes are taken from Richstone et al. [16].

Galaxy	Reissner - Nordstrom $\Delta T_{2,1}$			
	$q = 0.1$	$q = 0.2$	$q = 0.3$	$q = 0.4$
NGC4486 (M87)	148.3 h	145.4 h	140.1 h	131.7 h
NGC3115	89.9 h	88.1 h	84.9 h	79.8 h
NGC4374 (M84)	62.9 h	61.7 h	59.4 h	55.9 h
NGC4594 (M104)	44.9 h	44.0 h	42.4 h	39.9 h
NGC4486B (M104)	26.6 h	25.1 h	24.2 h	22.7 h
NGC4261	20.2 h	19.8 h	19.1 h	18.0 h
NGC4342 (IC3256)	17.5 h	17.2 h	16.6 h	15.6 h
NGC7052	14.8 h	14.5 h	14.0 h	13.2 h
NGC3377	8.1 h	7.9 h	7.6 h	7.2 h

TABLE III: Estimates for the time delay for the supermassive black hole located at the center of several nearby galaxies in the case of Reissner-Nordstrom spacetime geometry.

V. CONCLUSIONS

Gravitational lensing in the strong field limit may represent a key tool for the investigation of supermassive black holes. In principle, a complete characterization of the parameters of a black hole can be achieved by the study of the images formed by gravitational lensing of a background source. Technically, this study requires resolutions one or two orders of magnitudes better than actual VLBI projects, so that it stands as a possible observational target for the next future.

In this work we have pointed out that photons contributing to different strong field images take different times to reach the observer. This time delay is of order of few seconds for the black hole at the center of our Galaxy, but amounts to several days for more massive black holes at the centers of nearby galaxies.

If the background source is characterized by an intrinsic variability, it would then be possible to measure the time delay between different strong field images, with the important advantage of gaining one more indepen-

Galaxy	Janis-Newman-Winicour $\Delta T_{2,1}$			
	$\gamma = 0.9$	$\gamma = 0.8$	$\gamma = 0.7$	$\gamma = 0.6$
NGC4486 (M87)	132.8 h	116.0 h	98.7 h	80.5 h
NGC3115	80.5 h	70.3 h	59.8 h	48.8 h
NGC4374 (M84)	56.3 h	49.2 h	41.9 h	34.1 h
NGC4594 (M104)	40.2 h	35.2 h	29.9 h	24.3 h
NGC4486B (M104)	22.9 h	20.0 h	17.1 h	13.9 h
NGC4261	18.1 h	15.8 h	13.5 h	11.0 h
NGC4342 (IC3256)	15.7 h	13.7 h	11.7 h	9.5 h
NGC7052	13.3 h	11.6 h	9.9 h	8.0 h
NGC3377	7.2 h	6.3 h	5.4 h	4.4 h

TABLE IV: Estimates for the time delay for the supermassive black hole located at the center of several nearby galaxies in the case of Janis-Newman-Winicour spacetime geometry.

dent observable. The time delay is connected with the metric functions and thus can be used as a further source of information on the nature of the black hole. This result encourages our belief that gravitational lensing in the strong field limit stands as an interesting (maybe powerful) method for the classification of black holes.

Acknowledgments

The authors are grateful to Gaetano Scarpetta for helpful comments on the manuscript. V.B. whishes to thank the theoretical division of CERN and the Institute of Theoretical Physics of Zürich University for their hospitality.

[1] F.W. Dyson, A.S. Eddington, C. Davidson, *Phil. Trans. Roy. Soc.* **220A**, 291 (1920).
[2] P. Schneider, J. Ehlers, E.E. Falco, *Gravitational lenses*, Springer-Verlag, Berlin (1992).
[3] K.S. Virbhadra, G.F.R. Ellis, *Phys. Rev. D* **62**, 084003 (2000).
[4] S. Frittelli, T.P. Kling, E.T. Newman, *Phys. Rev. D* **61**, 064021 (2000).
[5] R.J. Nemiroff, *Amer. Jour. Phys.* **61**, 619 (1993).
[6] V. Bozza, S. Capozziello, G. Iovane, G. Scarpetta, *Gen. Rel. and Grav.* **33**, 1535 (2001).
[7] E.F. Eiroa, G.E. Romero, D.F. Torres, *Phys. Rev. D* **66**, 024010 (2002).
[8] A.O. Petters, *MNRAS* **338**, 457 (2003).
[9] V. Bozza, *Phys. Rev. D* **66**, 103001 (2002).
[10] V. Bozza, *astro-ph/0210109*, in press on *Phys. Rev. D*.
[11] S. Refsdal, *MNRAS* **128**, 307 (1964).
[12] R.D. Blandford, R. Narayan, *Ann. Rev. Astron. & Astrophys.* **30**, 311 (1992).
[13] D. Walsh, R.F. Carswell, R.J. Weymann, *Nature* **279**, 381 (1979).
[14] A. Janis, E. Newman, J. Winicour, *Phys. Rev. Lett.* **20** (1968) 878; M. Wyman, *Phys. Rev. D* **24** (1985) 839; R. Gautreau, *Nuovo Cimento B* **62** (1969) 360.
[15] ARISE web page: arise.jpl.nasa.gov; MAXIM web page: maxim.gsfc.nasa.gov; J.S. Ulvestad *astro-ph/9901374*.
[16] D. Richstone et al., *Nature* **395**, A14 (1998).